The accuracy of dose calculations by anisotropic analytical algorithms for stereotactic radiotherapy in nasopharyngeal carcinoma

2011 Phys. Med. Biol. 56 397

(http://iopscience.iop.org/0031-9155/56/2/008)

Phys. Med. Biol. **56** (2011) 397–413 doi:10.1088/0031-9155/56/2/008

The accuracy of dose calculations by anisotropic analytical algorithms for stereotactic radiotherapy in nasopharyngeal carcinoma

M W K Kan[1,2,3], J Y C Cheung[1], L H T Leung[1], B M F Lau[1] and P K N Yu[2]

[1] Department of Oncology, Princess Margaret Hospital, Hong Kong SAR, People's Republic of China
[2] Department of Physics and Materials Science, City University of Hong Kong, Tat Chee Avenue, Kowloon Tong, Hong Kong SAR, People's Republic of China

E-mail: kanwkm@ha.org.hk

Received 14 May 2010, in final form 5 November 2010
Published 22 December 2010
Online at stacks.iop.org/PMB/56/397

Abstract

Nasopharyngeal tumors are commonly treated with intensity-modulated radiotherapy techniques. For photon dose calculations, problems related to loss of lateral electronic equilibrium exist when small fields are used. The anisotropic analytical algorithm (AAA) implemented in Varian Eclipse was developed to replace the pencil beam convolution (PBC) algorithm for more accurate dose prediction in an inhomogeneous medium. The purpose of this study was to investigate the accuracy of the AAA for predicting interface doses for intensity-modulated stereotactic radiotherapy boost of nasopharyngeal tumors. The central axis depth dose data and dose profiles of phantoms with rectangular air cavities for small fields were measured using a 6 MV beam. In addition, the air–tissue interface doses from six different intensity-modulated stereotactic radiotherapy plans were measured in an anthropomorphic phantom. The nasopharyngeal region of the phantom was especially modified to simulate the air cavities of a typical patient. The measured data were compared to the data calculated by both the AAA and the PBC algorithm. When using single small fields in rectangular air cavity phantoms, both AAA and PBC overestimated the central axis dose at and beyond the first few millimeters of the air–water interface. Although the AAA performs better than the PBC algorithm, its calculated interface dose could still be more than three times that of the measured dose when a $2 \times 2\ \text{cm}^2$ field was used. Testing of the algorithms using the anthropomorphic phantom showed that the maximum overestimation by the PBC algorithm was 20.7%, while that by the AAA was 8.3%. When multiple fields were used in a patient geometry, the dose prediction errors of

[3] Author to whom any correspondence should be addressed.

the AAA would be substantially reduced compared with those from a single field. However, overestimation of more than 3% could still be found at some points at the air–tissue interface.

(Some figures in this article are in colour only in the electronic version)

1. Introduction

Radiotherapy is the principal treatment for nasopharyngeal carcinomas (NPCs). Recent experience has shown that when compared with conventional two-dimensional radiotherapy and three-dimensional conformal radiotherapy, the use of intensity-modulated radiation therapy (IMRT) for treating NPC can produce superior dose coverage of the primary tumors and a significant reduction of dose to the critical normal organs, including the spinal cord, temporal lobes and the parotids (Cheng *et al* 2001, Hunt *et al* 2001, Kam *et al* 2002). IMRT should be used as the standard technique for NPC radiotherapy whenever resources are available. In addition, NPC with local persistence after primary radiotherapy carries a high risk of treatment failure. Some investigators have shown that the use of stereotactic radiotherapy (SRT) boost after external radiotherapy in NPC is very effective in eradicating a persistent local disease (So *et al* 2002, Yau *et al* 2004). Stereotactic boost of 6–15 Gy after 60–66 Gy of external radiotherapy could also result in excellent local control for patients with NPC (Fu *et al* 2002, Hara *et al* 2008). Recently, the intensity modulation technique has been commonly used for both external radiotherapy and SRT boost. The target volume of NPC is located near air cavities, including the sphenoid sinus, the maxillary sinus, oral cavity and nasal cavity. The delivery of intensity-modulated beams in patients with NPC often involves the use of many small field segments passing through air cavities, especially for SRT boost in which the jaw sizes used are usually small, for which the segments are even smaller. The use of small fields in air cavities always leads to the electronic disequilibrium effect near the air–tissue interface that cannot be accurately accounted for in most of the algorithms of a commercially available clinical treatment planning system. Those algorithms that incorporate electron transport are mostly based on Monte Carlo-derived dose kernel superposition. Simplified density scaling of the kernels is applied for inhomogeneous media. Examples of these algorithms include the collapsed cone convolution (CCC) algorithm and the analytical anisotropic algorithm (AAA). Some studies have shown that even with the use of the above two algorithms, dose calculation errors can still occur beyond low-density media such as lung and air (Arnfield *et al* 2000, Martens *et al* 2002, Tillikainen *et al* 2008, Gray *et al* 2009). Arnfield *et al* (2000) showed that when a phantom with a 2 cm air gap was irradiated with a 4×4 cm^2, 6 MV beam, both the generalized Batho model and the Pinnacle's CCC model significantly over-predicted the dose on the air–tissue interfaces, relative to thermoluminescent dosimeter (TLD) measurement. Martens *et al* (2002) used an air cavity geometry of a 2 cm diameter tube to simulate the trachea and reported that the CCC algorithm overestimated the dose in the rebuild-up region by a maximum of 54% for a 10×1 cm^2 field. Tillikainen *et al* (2008) also detected limitations of the AAA in a lung equivalent slab phantom in the case of a small field size and large beam energy. Gray *et al* (2009) detected errors greater than 2.5% when the AAA was used to calculate the dose beyond a large air gap when using 10×10 cm^2 fields. Previous studies mainly investigated the effect of air cavities along the central axis, while the effect on the off-axis dose distribution was not clearly reported. The measurement of lateral profiles at and a few millimeters beyond the air–tissue interface could be used to demonstrate the increased lateral range of electron transport in air. The dose accuracy of the Eclipse's AAA at and near the air–tissue interfaces for small field sizes (smaller than 5×5 cm^2) has not been

previously reported. The aim of this study was to perform a comprehensive investigation on the accuracy of the Eclipse's AAA in predicting the dose effects due to air gaps for small fields from a 6 MV beam. The field sizes used a range from 2×2 to 5×5 cm^2. Both central axis depth dose distributions and lateral dose profiles at and a few millimeters beyond the air–tissue interfaces of rectangular air cavities were calculated by the AAA and then compared with those calculated by the pencil beam convolution (PBC) algorithm, EGS Monte Carlo simulations and measurements. The dependence of the dose calculation accuracy on the cavity size, field size and depth was reported. Although there can be dose inaccuracies predicted by the algorithms for single small fields, the dose calculation error can be substantially reduced in clinical patient plans where the anatomical structures are much more complicated and the doses are delivered by several intensity-modulated fields from different directions. Bragg *et al* (2008) verified the doses calculated by the AAA from IMRT nasopharynx plans using a head and neck phantom containing bone and air inhomogeneities. They showed that the discrepancies were mostly within 3% or 3.5 mm. However, the points selected for measurement might not be exactly at air–tissue interfaces. In our work, measurements with an anthropomorphic phantom were performed to assess the accuracy of the dose calculations by the AAA and PBC algorithm at the air–tissue interface in clinical situation, in which the technique of intensity modulation was used for SRT. The NP region of the anthropomorphic phantom was specially modified to simulate that of a typical NP patient. TLD inserts were tailor-made at air–tissue interfaces of the nasal cavities and oral cavities, so that the doses could be measured and compared with the dose calculations.

2. Materials and methods

2.1. Measurement of the central axis depth dose and lateral profiles

The central axis depth dose data of phantoms with rectangular air cavities were taken for a 6 MV beam from a Varian Clinac 6EX accelerator (Varian Medical Systems, Palo Alto, CA). Two rectangular phantoms with different sizes of rectangular air cavities were used in this study. The first phantom consisted of a $5 \times 5 \times 30$ cm^3 rectangular air cavity, which was sandwiched between 5 cm of solid water (Gammex-RMI, Middleton, WI) above and 15 cm of solid water below. Slabs of rectangular perspex were sandwiched between the solid water to create the air cavity, as shown in figure 1. The second phantom was constructed in the same way as the first one, except that the size of the air cavity was reduced to $3 \times 3 \times 30$ cm^3. Measurement of the central axis depth dose data was performed with a Markus parallel plate ionization chamber (PTW/advanced Markus chamber, Type TN34045, PTW, Freiburg, Germany) and TLDs. The isocenter was set at 1 cm below the distal surface of the air cavity. The field sizes used were 2×2, 3×3 and 5×5 cm^2. Thin TLD-100 chips (Harshaw, Erlangen, Germany) with size $3.2 \times 3.2 \times 0.381$ mm were used. In order to reduce statistical errors, all reported data were taken as the average of four individual measurements. All the measured data were taken relative to a dose of 100 cGy at the depth of maximum dose in a homogeneous solid water phantom irradiated with a 10×10 cm^2 field. Systematic uncertainties in dose measurements by the advanced Markus chamber may exist near the air–tissue interfaces due to scatter of secondary electrons from the side walls. Besides, taking measurement at the proximal interface with the Markus chamber requires the chamber to be turned upside down. Therefore, in additions to thin TLDs, radiochromic films (Gafchromic EBT, International Specialty Products, NJ, USA) were used to measure the interface doses on the central axis. They were chosen for the measurement because the effective atomic number of the EBT film

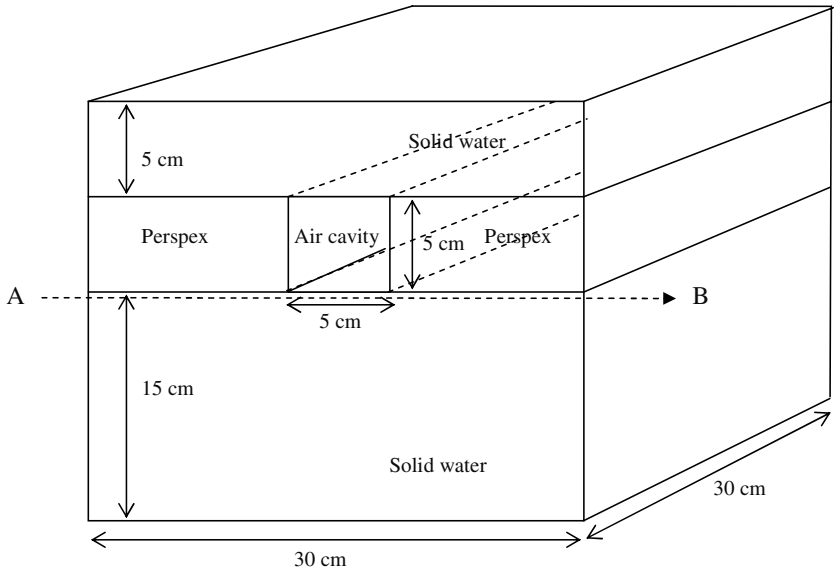

Figure 1. The 5 × 5 × 30 cm^3 rectangular air cavity phantom for depth dose and dose profile measurement from single small fields.

is 6.84, which is near tissue equivalent. The manufacturer indicated that the films would have less than 10% response difference between MeV and KeV photon. The films were measured with an Epson V700 (Epson, Suwa, Nagano) flat bed scanner. The response in a red color channel was used for dosimetry. Due to the possibility of non-uniformity of response of the scanner over the scan field, especially in regions about 2–3 cm from the left and right edges, the films were all positioned in the center of the scan area for measurement. Due to the effect of anisotropic light scattering, the pixel response of the scanner could be affected by the orientation of the film in the scanner; it is critical to always scan the films in the landscape orientation. The irradiated films were scanned 24 h after exposure. To perform film calibration, seven small film pieces were cut from the same sheet with marked orientation. They were placed horizontally on the central axis at 10 cm depth in solid water slabs and then were irradiated to different known doses to obtain the optical density to dose calibration curve. For measurement of central doses at both the distal and the proximal air–solid water interfaces, the films were cut into 3 × 3 cm^2 strips and placed on the central axis of the air cavity phantoms. Optical density data were only obtained near/at the center of the film. In addition, central axis depth dose distributions in the cavity phantom were also compared to the results from Monte Carlo simulations. The Monte Carlo system employed was the PRESTA (parameter-reduced electron-step transport algorithm) version of the EGS4 (electron gamma shower) computer code. Detailed descriptions on the structure of the EGS4 code can be found in Jenkins *et al* (1988). The phantom geometry was defined using macros of PLANE1 and PLAN2P of 'Code Geometry of EGS4' at HOWFAR subroutine (Nelson and Jenkins 1988, Rogers and Mohan 2000). The phantom medium was defined as solid water and cavity was defined as air. The dimensions of air cavity can be varied by adjusting the separation between plans, i.e. 5 × 5 × 30 and 3 × 3 × 30 cm^3. A 6 MV photon beam (Rogers and Mohan 2000) with a different field size was irradiated on the phantom at source to axis distance (SAD) = 100 cm. The field sizes used were 2 × 2, 3 × 3 and 5 × 5 cm^2. A percentage

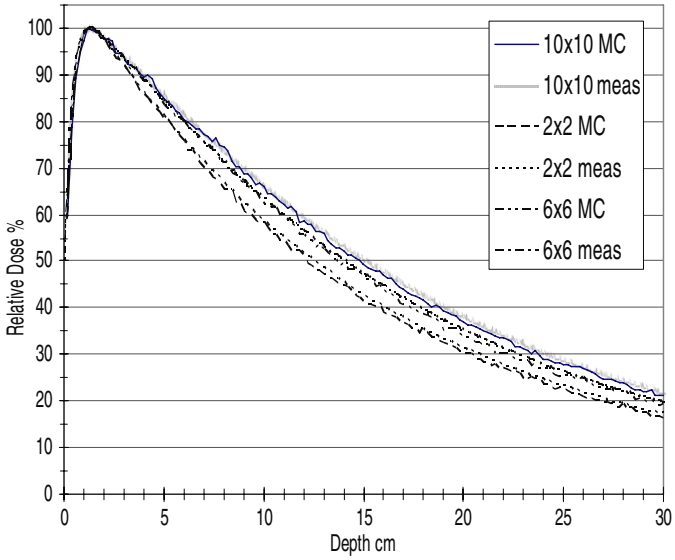

Figure 2. The Monte Carlo simulated and measured percentage depth dose curve in a homogeneous water phantom matches for various field sizes.

depth dose curve was obtained by energy depositions along scoring bins in the direction of the beam axis. The dimensions of the scoring bins were 1/10 the dimensions of the given field size with a bin thickness of 0.2 mm. The dimensions of scoring bins were small enough to give a high resolution of the dose profiles and were large enough to give good statistical results. To achieve good statistical accuracy, the number of histories followed was 2.0×10^8. The standard error of about 2% was obtained. The cutoff energies for electrons and photons were set to be 0.521 MeV (rest mass of electron + 0.01 MeV) and 0.01 MeV, respectively. High cutoff energies shortened the simulation time at the expense of reliable results. In our study, further lowering these cutoff energies caused no observable differences of the output results. As shown in figure 2, the Monte Carlo simulated percentage depth dose curve in a homogeneous water phantom matched with our measurement results to within 2% for various field sizes.

The lateral profiles at the distal interface, 1 and 3 mm beyond the air cavity, were also measured with the radiochromic films for the two cavity sizes from 2×2 to 5×5 cm^2 fields. The films were cut such that they were at least a few centimeters larger than the field dimension. The lateral profiles were scanned along the direction from A to B, as shown by the dashed line in figure 1.

2.2. Dose calculations

The air cavity phantoms were scanned with a GE LightSpeed RT 16-multislice CT simulator (GE Health, Waukesha, WI) using the protocol of our clinic for head and neck scans (120 kV, 300 mA, and 2.5 mm slice thickness). AAA calculations were performed with the Eclipse TPS version 8.6 (Varian Medical Systems, Palo Alto, CA) for the scanned phantoms, so that heterogeneous correction was done using the CT numbers of the actual materials.

The AAA is one of the models that incorporate electron transport for dose calculation. It is a three-dimensional PBC/superposition algorithm that uses Monte Carlo-derived scatter

kernels to model primary photons (primary source), scattered extra focal photons and electrons scattered from the beam limiting devices (electron contamination source). The primary source is the point source located at the target plane. It models the bremsstrahlung photons created in the target that do not interact in the treatment head. The extra-focal source is a Gaussian plane source located at the bottom plane of the flattening filter. It models the photons that result from interactions in the accelerator head outside the target, primarily in the flattening filter, primary collimators and secondary jaws. Electron contamination is modeled with a depth-dependent curve that describes the total amount of electron contamination at a certain depth. The final dose distribution is computed by the superposition of the dose calculated by the photons and electron convolutions. The kernels are calculated using a sum of six depth-dependent weighted exponentials, defining the lateral scattering in order to fit the Monte Carlo-derived pencil beam scatter. To account for the presence of inhomogeneities, simple density scaling of the kernels is applied. Secondary electron transport is only modeled macroscopically. The electrons are assumed to travel in straight lines. The depth and lateral components are independently scaled, i.e. the particles are first assumed to arrive at the plane of destination along the central line of the beamlet and then scatter to the destination voxel in the lateral direction. As a result, divergent scatter is not always correctly taken into account. Using the above assumption, the algorithm cannot predict the gradual build-up and build-down effects near heterogeneous interfaces. The AAA uses a separate build-up kernel in the form of a dual exponential function to account for the changes in electronic equilibrium across the interfaces of heterogeneities and water. A more detailed description of the algorithm can be found in Tillikainen *et al* 2008.

The geometry of the dose calculation grid used by the AAA is divergent such that the dimension of the beamlet is matched to the dose calculation grid size. The Eclipse system allows for calculating dose distributions for grid sizes ranging from 1 to 5 mm. All calculations in this work were performed with a grid size of 2.5 mm, as this is the internal grid size used by Eclipse to compute and store fluence. It is also the default value that we used in dose calculations for clinical head and neck cases. In addition, the calculations of central axis depth dose data of a 3×3 cm^2 field in a homogeneous solid water phantom and the $5 \times 5 \times 30$ cm^3 air cavity phantom were repeated for grid sizes of 1, 2, 3, 4 and 5 mm to study the effect of grid size on dose calculation.

For comparison, calculations were also performed with the PBC algorithm, which is also available with the Eclipse TPS. All calculations by the PBC algorithm were performed with a grid size of 2.5 mm. The method of inhomogeneous correction used by the PBC algorithm was the modified Batho power law (MB). The Batho method is an empirical correction that uses tissue-maximum ratio for high-energy beams, raised to a power that depends on the median's electron density relative to water. This method does not incorporate electron transport and is unable to adequately account for the effect of lateral electron transport in and near inhomogeneities.

2.3. Anthropomorphic measurements

The air–tissue interface doses from six different intensity-modulated stereotactic radiotherapy (IMST) boost plans were measured in an anthropomorphic phantom (the RANDO phantom, The Phantom Laboratory, Salem, NY), as shown in figure 3(a). The planning target volume (PTV) ranged from 20.6 to 56.7 cm^3 with a mean of 34.3 cm^3. The jaw sizes ranged from about 3×3 to 6×6 cm^2, depending on the size of the individual target. The original RANDO phantom did not include any nasal cavity and recess at the air–tissue interfaces for holding TLD-100 chips (Harshaw, Erlangen, Germany). The phantom was therefore modified to simulate the NP region of a typical patient as shown in figures 3(b) and (c). Four TLD

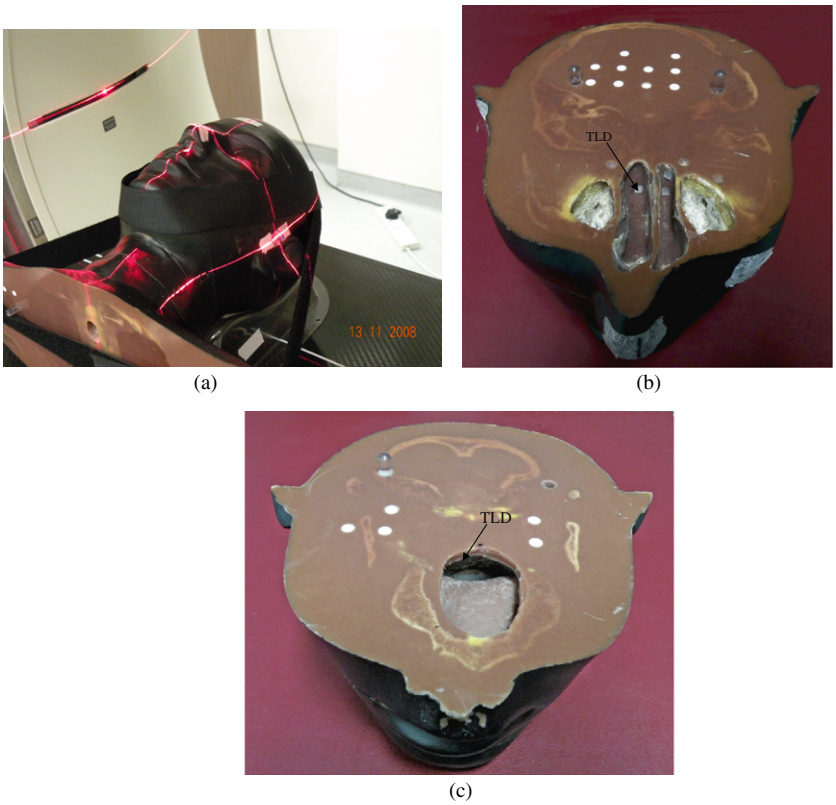

Figure 3. Air–tissue interface doses from intensity-modulated SRT plans were measured in (a) the anthropomorphic phantom. (b) TLDs were placed at the air–tissue interface in the nasal cavities near the NP region. (c) The TLD was placed at the air–tissue interface in the oral cavity.

recesses were made at the air–tissue interfaces in the nasal cavities and one TLD recess was made in the oral cavity. The size of the recesses was set such that the TLD chips were tightly fitted and held firmly at the air–tissue interfaces during the measurement.

The head and shoulder of the RANDO phantom were scanned with a GE LightSpeed RT 16-multislice CT simulator (GE Healthcare, Waukesha, WI) using the protocol used in our clinic for head and neck scans (120 kV, 300 mA, and 2.5 mm slice thickness). Before the CT scan, the position of the phantom was adjusted so that the laser alignment centers were near the NP region. Reference markers were taped to the phantom surface for marking the origin of the CT scans, as shown in figure 3(a). The intensity-modulated stereotactic boost radiotherapy planning parameters of six previously treated patients, including the beam directions, jaw sizes, and the fluence maps, were transferred to the CT image set of the RANDO phantom, the location of the isocenter was then adjusted so that it was near the NP region and the fields covered all the five tailor-made TLD recesses. The original prescribed dose to the target volume was 18 Gy in three fractions. In order to perform all the measurements within the linear dose response range of the TLD-100 chips, the prescribed dose was reduced to 0.8 Gy per fraction, dose calculation was then performed for each planning case with both the PBC algorithm and the AAA. About seven to ten fields were used for each plan. Before the actual

phantom measurements were made, the whole set of TLD chips were irradiated with a known dose using a standard calibration field setup for the 6 MV x-ray beam. Each TLD chip was assigned a sensitivity value that related its individual dose response to the mean dose response of the set. The sensitivity value was taken as the average of three irradiations. Assigning a sensitivity correction factor to each TLD chip could improve the accuracy of our measurement. During the actual measurement, the phantom for each patient plan was repeated five times and the average value was taken to reduce statistical errors. The measured dose data were then compared with those calculated by the PBC algorithm and AAA.

3. Results

3.1. Depth dose data

Figures 4(a)–(f) show the measured and calculated depth dose data in both the $5 \times 5 \times 30$ and the $3 \times 3 \times 30$ cm^3 air cavity phantoms for 2×2, 3×3 and 5×5 cm^2 fields of the 6 MV beam. When looking at the rebuild-up region beyond the air cavity, it can been seen from the depth dose data that the measurement results by TLD were closely matched with those measured by the Markus ion chamber and those simulated by Monte Carlo. All measured data demonstrated that the rebuild-up mainly occurred at the first 1 cm beyond the air cavity. Quantitative comparison of the rebuild-up effect measured by TLD beyond the air cavity was done by using the formalism of Epp *et al* (1977), who defined the inverse of the build-up ratio (BUR^{-1}) as the ratio of the dose measured at the interface to the dose measured at the depth of maximum rebuild-up. For the $5 \times 5 \times 30$ cm^3 air cavity, the BUR^{-1} increased from 0.25 to 0.53 as the field size increased from 2×2 to 5×5 cm^2, while for the $3 \times 3 \times 30$ cm^3 air cavity, the BUR^{-1} increased from 0.34 to 0.91. The rebuild-up effect increased with decreasing field sizes and was more severe for the larger air cavity. The depth dose data estimated using the PBC algorithm did not show any rebuild-up beyond the air cavity for all field sizes and cavity sizes. Its calculated results after the rebuild-up region matched well with the measured results. For the AAA, the calculated results did predict some rebuild-up beyond the distal interface. However, it significantly underestimated the rebuild-up effect for all small field sizes. The BUR^{-1} predicted by the AAA only ranged from 0.88 to 0.93 and from 0.92 to 0.99 beyond the larger air cavity and the smaller air cavity respectively as the field sizes increased from 2×2 to 5×5 cm^2. A summary showing both measured and calculated interface doses and their discrepancies is given in table 1. The interface doses measured by TLD and radiochromic film were quite close to each other. It can be seen that although the AAA produced considerably more accurate results than the PBC algorithm, it still overestimated the distal interface doses significantly for small field sizes especially for the 2×2 and 3×3 cm^2 fields. For 2×2 cm^2, the overestimation at the distal interface was 265% and 179% respectively for the larger cavity phantom and for the smaller cavity phantom. For 3×3 cm^2, it was 163% and 94% respectively for the larger cavity phantom and for the smaller cavity phantom. On the other hand, the measured build-down effect above and close to the proximal interface was small. It only occurred near the first 2–3 mm adjacent to the proximal interface. Both the PBC algorithm and the AAA hardly predicted any build-down effect. The overestimation of doses near the proximal end for the smallest measured field size was 8% and 11% by the AAA and the PBC algorithm respectively. The magnitude of overestimation was very close for both cavity sizes.

Figures 5(a) and (b) show how the grid size affects the performance of AAA in a slab-type phantom with and without air cavity using a 3×3 cm^2 field. It can be seen from figure 5(a) that in the homogeneous water phantom, the change of grid size from 1 to 5 mm had negligible

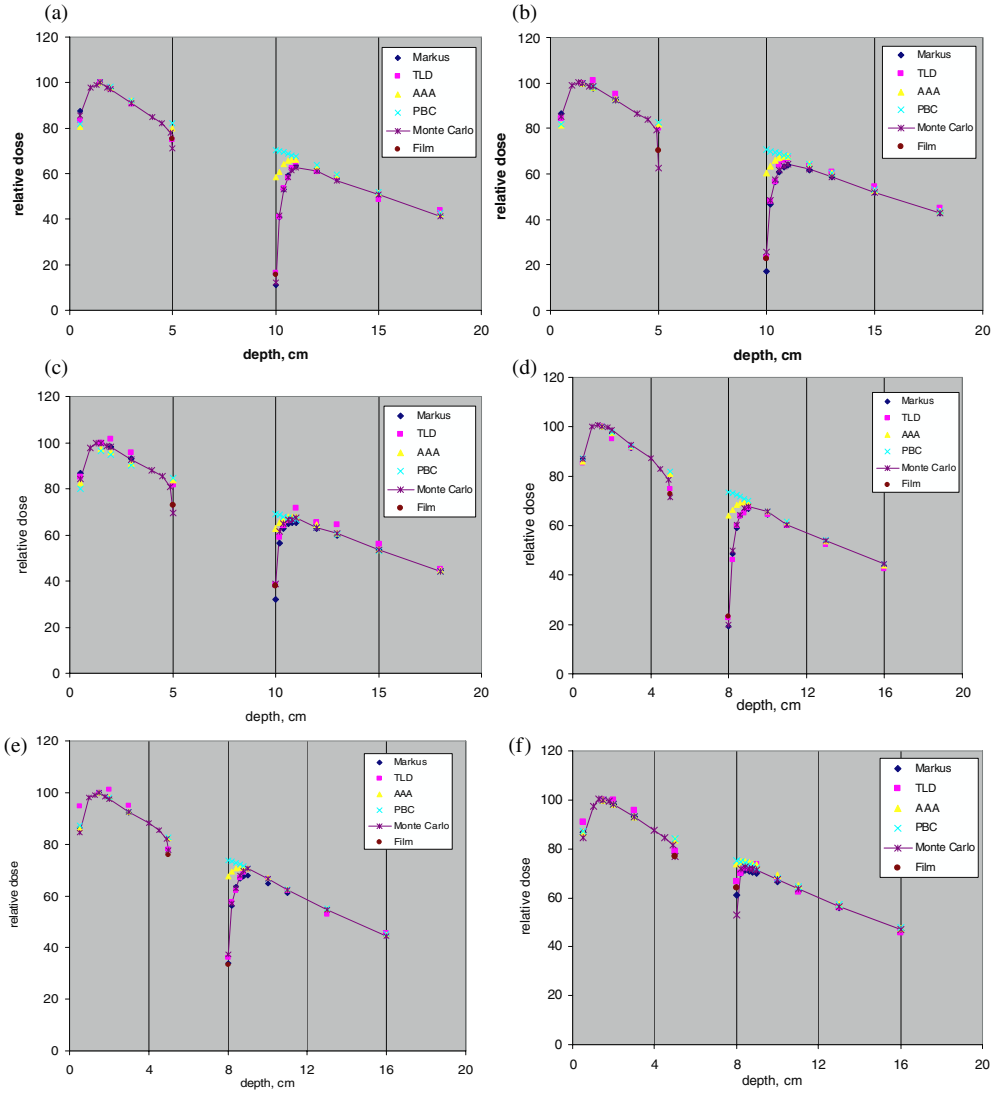

Figure 4. The depth dose data measured by TLDs, Markus chamber and radiochromic films were compared to depth dose data calculated by the AAA, the PBC algorithm and Monte Carlo simulations in the $5 \times 5 \times 30$ cm^3 air cavity phantoms for (a) 2×2, (b) 3×3 and (c) 5×5 cm^2 fields, and also in the $3 \times 3 \times 30$ cm^3 air cavity phantoms for (d) 2×2, (e) 3×3 and (f) 5×5 cm^2 fields of the 6 MV beam.

effect on the calculation results. For the calculation in the air cavity phantom, the results were very close for grid sizes ranging from 2 to 5 mm. However, the data calculated using the 1 mm grid deviated from those of the others by 2–3%. Since the depth dose calculated using the 2.5 mm grid was previously verified by measurement as shown in figure 4(b) to be accurate except the first few millimeters beyond the air cavity, doses calculated using the 2–5 mm grid should be reliable.

Table 1. A summary showing the discrepancies of air–solid water interface doses between calculations by the Eclipse treatment planning system and measurement for the air cavity phantoms using a 6 MV beam.

Field size ($cm^{2)}$	Position	TLD (cGy)	Film (cGy)	AAA cal. dose (cGy)	PBC cal. dose (cGy)	AAA-measured data[a] (%)	PBC-measured data[a] (%)
For air cavity $5 \times 5 \times 30$ cm^3							
2×2	Proximal interface	74.8 ± 1.4	75.2 ± 2.21	80.0	82.0	6.7	9.3
	Distal interface	16.3 ± 0.28	15.8 ± 0.4	58.6	70.4	265.1	338.6
3×3	Proximal interface	72.3 ± 1.8	70.2 ± 1.96	81.9	82.7	14.9	16.1
	Distal interface	23.3 ± 0.54	22.7 ± 0.71	60.6	70.6	163.5	207.0
5×5	Proximal interface	74.8 ± 1.92	72.8 ± 1.46	84.0	84.6	13.8	14.6
	Distal interface	38.2 ± 0.98	37.9 ± 1.35	62.8	68.9	65.1	81.1
For air cavity $3 \times 3 \times 30$ cm^3							
2×2	Proximal interface	74.7 ± 1.64	72.9 ± 2.45	80	81.9	8.4	11.0
	Distal interface	22.6 ± 0.79	23.2 ± 0.82	64	73.6	179.5	221.4
3×3	Proximal interface	78.0 ± 2.03	76.0 ± 2.11	82.4	82.8	7.0	7.5
	Distal interface	36.2 ± 1.02	33.4 ± 1.36	67.6	73.9	94.3	112.4
5×5	Proximal interface	79.2 ± 1.89	76.7 ± 2.21	83.9	84.3	7.6	8.1
	Distal interface	66.4 ± 1.67	64.2 ± 1.93	74.0	75.3	13.3	15.3

[a] Measured data refer to the mean of TLD and film measurements.

3.2. Profiles

Figures 6(a)–(c) show the calculated and measured profiles at the distal interface, 1 and 3 mm beyond the $5 \times 5 \times 30$ cm^3 air cavity for the 2×2 cm^2 field. Looking at the measured dose profiles, it was found that the central doses were much lower than those predicted by the calculations, while the measured doses outside the field edge were higher than those predicted by the calculation. This must be due to the increased lateral range of secondary electrons traveling through the air cavity. Some of those electrons generated inside the field and near the field center had their energy deposited in the tails of the profile outside the field edge. This effect due to lateral electronic equilibrium decreased significantly with depth beyond the air cavity. This can be shown by comparing the profiles at the interface to those at 3 mm depth. When comparing the AAA and PBC algorithm calculated profiles, it was found that although the one predicted by the AAA had lower central doses than that predicted by the PBC algorithm, their tails almost overlapped with each other. This proves that both algorithms do not predict the lateral transport of secondary electrons correctly from the air cavity.

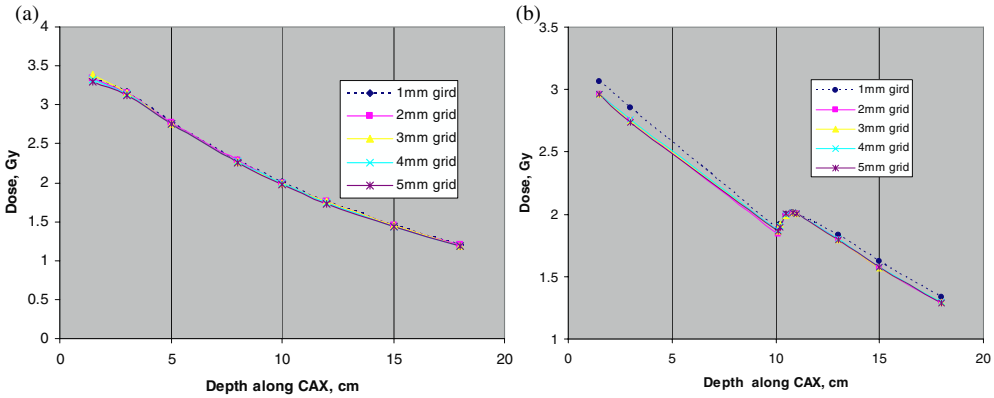

Figure 5. The depth dose data calculated by the AAA using grid sizes 1, 2, 3, 4 and 5 mm using 3 × 3 cm^2 field in (a) a homogeneous solid water phantom and (b) in the 5 × 5 × 30 cm^3 air cavity phantoms.

Figures 7(a)–(c) show the profiles of the same air cavity for the 3 × 3 cm^2 field. A similar trend could be observed as for the 2 × 2 cm^2 field; it was only that the effect of lateral electron transport was smaller and therefore the predicted dose profiles were relatively closer to the measured ones. Figures 8(a)–(c) show the calculated and measured profiles beyond the smaller air cavity (3 × 3 × 30 cm^3) for the 2 × 2 cm^2 field. The measured profiles also illustrated the effect of lateral electronic equilibrium.

3.3. Anthropomorphic interface measurements

Table 2 shows the air–tissue interface doses at five different positions within the anthropomorphic head and neck phantom using six different SRT treatment plans. The isocenter of each plan was adjusted so that all five positions were included in the treatment fields. Position 1 was located in the oral cavity as shown in figure 3(c). The average volume of the oral air cavity irradiated by the 6 MV beams was around 20 cm^3. The lateral width was about 3 cm, the anterior–posterior length was about 6 cm and the longitudinal depth was about 1–1.5 cm. Positions 2–5 were located in the nasal cavity as shown in figure 3(b). The volume of the nasal cavity irradiated by the beams ranged from 20 to 30 cm^3. The lateral width was about 2 cm, the anterior–posterior length was about 5 cm and the longitudinal depth was about 2–3 cm. Columns VI and VII of table 2 show the percentage differences between the measured and calculated doses. The quadratic mean (QM) of the percentage errors of the five points predicted by the PBC algorithm for each patient plan ranged from 5.6% to 12.7%, while that for the AAA only ranged from 1.1% to 4%. The maximum overestimation by the PBC algorithm was up to 20.7% occurred in the oral cavity for patient 1, while that by the AAA was 8.3% occurred exactly at the same position of the same plan. The maximum discrepancy between the PBC calculated dose and the measured dose also occurred at position 1 in the oral cavity for patient plan 2 and 3. The overestimations by the AAA were significantly reduced when compared with those by the PBC algorithm. Despite of the fact that there were large discrepancies between the AAA calculated and measured depth dose data along the central axis at/near the air–tissue interface from single small fields, the maximum discrepancy predicted by the AAA as compared to the measured interface dose for the composite multiple directional IMRS plans was only 8.3%.

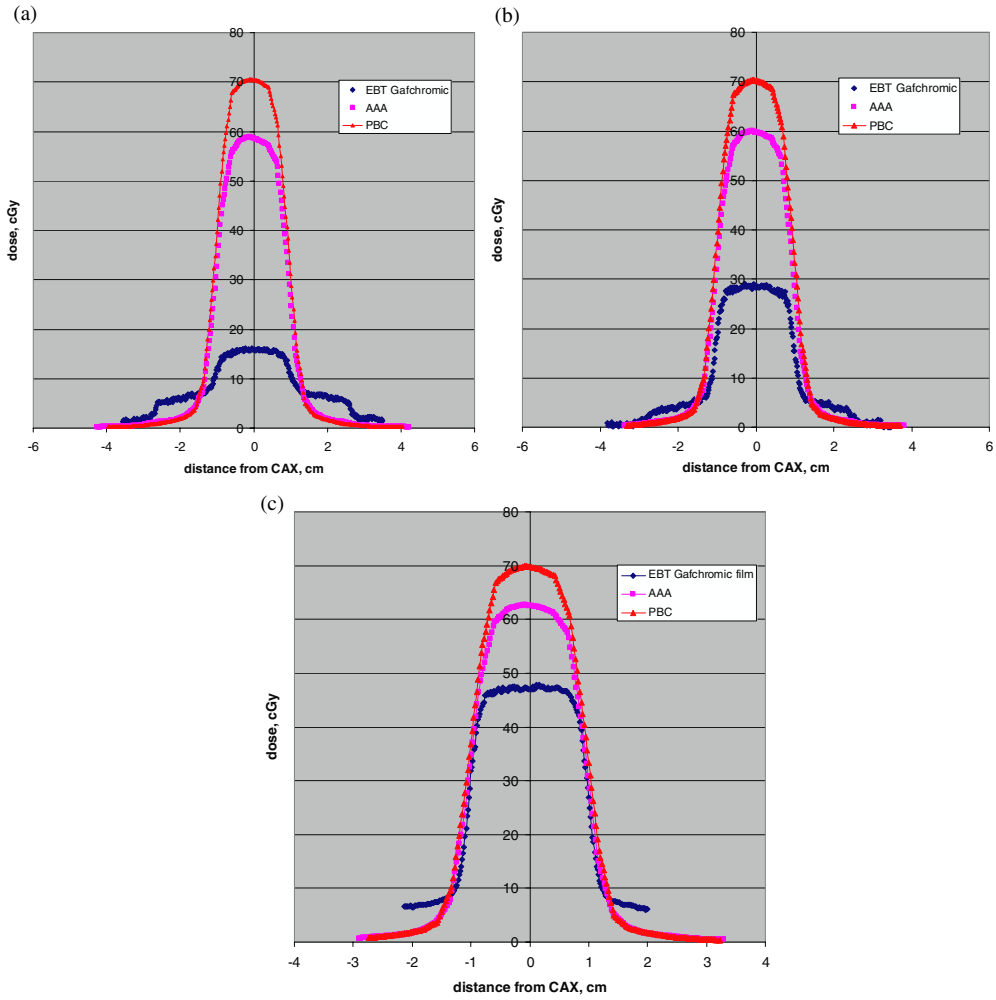

Figure 6. The calculated and measured profiles at (a) the distal interface, (b) 1 mm and (c) 3 mm beyond the 5 × 5 × 30 cm^3 air cavity for the 2 × 2 cm^2 field.

4. Discussions

The AAA implemented in Varian Eclipse was developed to replace the PBC algorithm for more accurate dose prediction in an inhomogeneous medium especially with the involvement of a low-density medium. Many investigators have shown that the AAA calculation produced more accurate dose prediction than that of the PBC algorithm in lung and at the interface between lung and tissue for 6 MV beams using small fields (Van Esch *et al* 2006, Ding *et al* 2007, Sterpin *et al* 2007, Tillikainen *et al* 2008). Our study is focused on the testing of dose prediction accuracy close to the air–tissue interface in phantoms with large air cavities. From the results of the depth dose data measurements and dose profile measurements, it was found that although the AAA performed better than the PBC algorithm as it predicted some secondary build-up beyond the air cavity, its predicted secondary build-up was of a much smaller extent than the actual measurement in the first few millimeters beyond the air cavity,

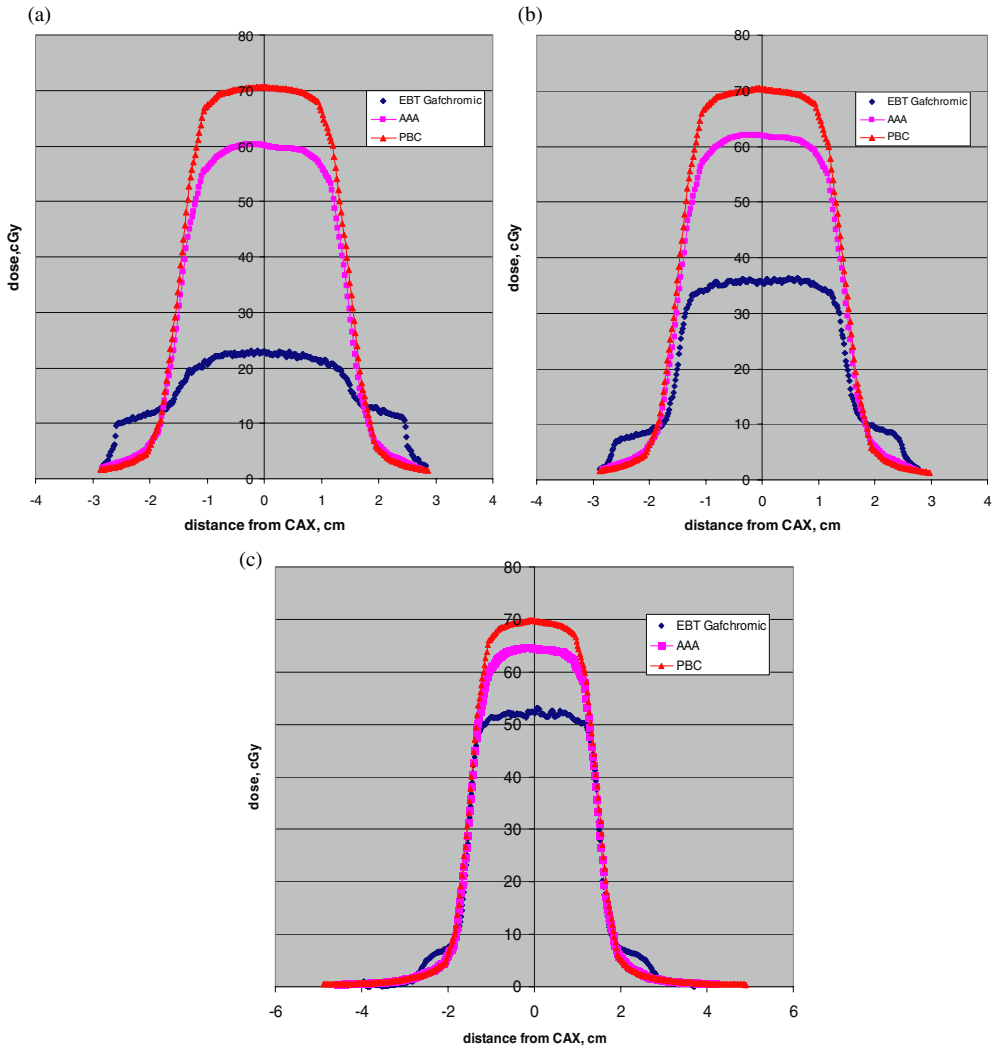

Figure 7. The calculated and measured profiles at (a) the distal interface, (b) 1 mm and (c) 3 mm beyond the 5 × 5 × 30 cm^3 air cavity for the 3 × 3 cm^2 field.

especially when using fields smaller than 5 × 5 cm^2. For the most extreme case, i.e. when a 2 × 2 cm^2 field was used to irradiate the phantom with a 5 × 5 × 30 cm^3 air cavity, the AAA estimated dose at the distal interface could be 265% more than the measured dose. There were also large discrepancies between the calculated and measured dose profiles as shown in figure 6, illustrating that the AAA did not model the effect of lateral electronic disequilibrium properly in some extreme cases. For heterogeneity correction, the AAA assumes that the depth-directed and lateral components can be independently scaled. The depth-dependent component is scaled by taking into account the radiological distance between the surface and the calculation points. For the scaling of the scatter kernel, the water equivalent path length is calculated radially from the center of the beamlet. Therefore, it does not take into account correctly the divergent scatter of heterogeneities from upper levels. With the above

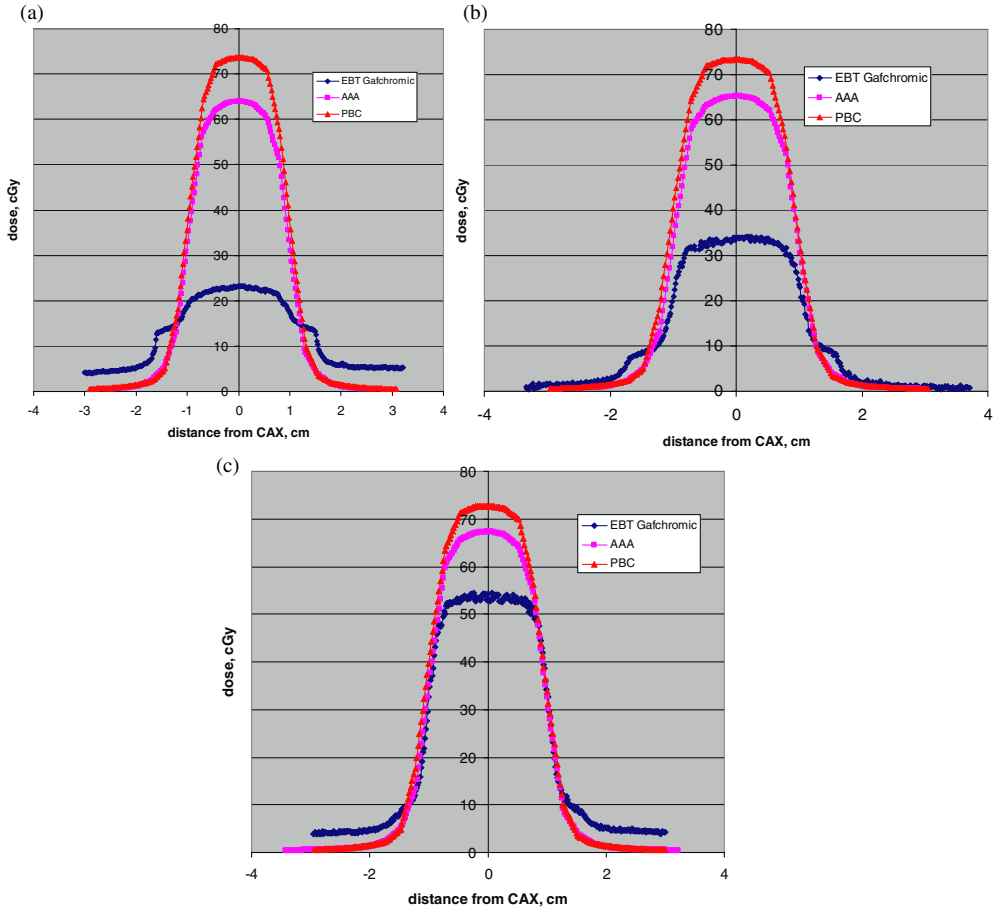

Figure 8. The calculated and measured profiles at (a) the distal interface, (b) 1 mm and (c) 3 mm beyond the 3 × 3 × 30 cm^3 air cavity for the 2 × 2 cm^2 field.

assumption it can produce desirable results only when calculating dose to a uniform phantom of non-water-equivalent electron density or in regions that are after a sufficient distance from the material interface. In the AAA, in order to predict the build-up and build-down transitions near interfaces, a forward build-up convolution kernel (k_b), which is a dual exponential function, is employed to the energy deposition. The free parameters in the formula are chosen such that the build-up effect between vacuum and water is preserved (Tillikainen *et al* 2008). However, our results show that in the case of a very large low-density medium and small field sizes, the use of this kernel k_b underestimates the build-up and build-down effects near the interfaces. The overestimation of doses increases with increasing air cavity size and with decreasing field size.

Such significant overestimation by the AAA was not found when a more clinical situation was simulated using the anthropomorphic phantom. From the results of anthropomorphic interface measurements, it was shown that the prediction error of interface doses by the AAA was not as significant as those predicted from single fields; a maximum overestimation of 8% occurred at a point in the oral cavity. The QM discrepancy over the five points between the measured doses and the predicted doses for the six plans was within 4%. For the PBC

Table 2. Air–tissue interface doses in the anthropomorphic phantom for the six intensity-modulated SRT plans using a 6 MV beam.

I	II	III	IV	V	VI	VII
Patient no	Position	AAA calculated dose (cGy)	PBC calculated dose (cGy)	TLD measured dose (cGy)	% diff. (AAA-measured)	% diff. (PBC-measured)
1	1	75.7	84.4	70.0 ± 3.2	8.3	20.7
	2	90.0	94.9	88.0 ± 1.1	2.3	7.9
	3	89.4	96.8	91.0 ± 1.7	−1.8	6.4
	4	94.4	97.6	93.0 ± 1.1	1.9	5.4
	5	93.9	98.2	93.0 ± 0.9	0.5	5.1
				QM[a]	4.0	10.8
2	1	63.3	70.9	59.0 ± 3.1	7.2	20.1
	2	80.8	86.9	77.7 ± 1.5	4.0	11.9
	3	81.7	88.1	81.9 ± 0.9	−0.2	7.6
	4	80.2	88.8	81.1 ± 1.2	−1.15	9.5
	5	80.7	87.4	78.8 ± 1.1	2.5	10.9
				QM	3.9	12.7
3	1	78.2	87.4	76.2 ± 2.1	2.6	14.7
	2	83.2	89.2	80.6 ± 1.1	3.2	10.6
	3	84.8	90.3	84.8 ± 1.0	−0.02	6.4
	4	82.6	90.0	80.4 ± 1.2	2.7	11.9
	5	82.7	88.0	81.7 ± 1.7	1.2	7.7
				QM	2.2	10.7
4	1	76.8	80.0	77.0 ± 0.4	−0.3	3.9
	2	80.6	85.2	80.1 ± 0.7	0.7	6.4
	3	81.7	86.7	81.9 ± 1.5	−0.2	5.9
	4	82.1	87.9	81.6 ± 1.0	0.6	7.7
	5	82.0	86	83.9 ± 0.5	−2.3	2.5
				QM	1.1	5.6
5	1	73.2	77.6	71.3.0 ± 1.3	2.7	8.9
	2	80.0	84.6	79.5 ± 2.1	2.6	8.5
	3	81.1	86.4	82.3 ± 0.7	−1.1	5.4
	4	77.6	84.5	74.0 ± 0.8	5.0	14.3
	5	80.3	86.9	80.7 ± 0.7	−1.0	7.2
				QM	2.9	9.3
6	1	78.8	86.8	77.1 ± 0.4	2.2	12.6
	2	82.4	88.3	82.6 ± 0.9	−0.3	6.9
	3	83.4	89.9	85.5 ± 0.6	−2.4	5.2
	4	81.5	88.5	77.7 ± 0.5	4.9	13.9
	5	82.1	89.0	83.1 ± 1.4	−1.2	7.1
				QM	2.7	9.8

[a] QM refers to the quadratic mean of the percentage differences for the five points of each plan.

algorithm, the calculated doses at all the investigated points of the six plans were higher than those of the corresponding points calculated by the AAA algorithm. The maximum overestimation was 20.7% by PBC which occurred at the same point of the same plan as that

by the AAA, while the mean overestimation of all the plans was 9%. The overestimations of interface doses by both algorithms for the six clinical plans were significantly reduced when compared with those of the single field measurements. First of all, the sizes of the nasal cavity (about 40 cc) and oral cavity (about 20 cc) were smaller than those of the rectangular air cavity phantom. The effect of lateral electronic disequilibrium decreases with decreasing air cavity size. Secondly, about seven to ten fields were used for each plan and each field was composed of a large number of segments; the overestimation along the central axis contributed from each single segment was significantly reduced for the composite plan. When looking at figures 6(a)–(c), the algorithms underestimated the doses outside field edges for the small fields. For each small segment, although the algorithms overestimate the dose along its central axis, there is a possibility that the doses contributed from the adjacent small segments might be underestimated due to lateral electronic disequilibrium, therefore compensating part of the overestimation. Summation of doses at a point contributed from beams coming from different directions further reduces the impact of the secondary build-up effect due to one single segment. Thirdly, the geometry of the anthropomorphic phantom was more complex than that of the rectangular air cavity phantoms. Some of the beams passed through some bony structures before reaching the air–tissue interface, making the interpretation of the results less obvious. In addition, the measurements in the anthropomorphic phantom were made with TLD-100 chips; the results were therefore averaged over the first 1 mm depth near the air–tissue interfaces. They were not exactly the doses at the interface.

5. Conclusions

Indirect modeling of secondary electron transport for the effects of inhomogeneities through the scaling of the scatter kernels and the scaling of scatter kernels only in the lateral and depth directions results in dose calculation errors by the AAA near and at air–tissue interfaces. Our study has shown that the prediction errors by the AAA could still be substantial near the first few millimeters beyond a large air cavity from a single small field of a 6 MV beam. Since the use of stereotactic radiotherapy boost after external radiotherapy in nasopharyngeal carcinoma is common for the treatment of persistent local disease, it is important to investigate the accuracy of both AAA and PBC algorithm in the various clinical scenarios. Based on the results of the anthropomorphic measurements, overestimation greater than 3% is possible by the AAA. The results from the AAA are much better than those calculated by the PBC algorithm. However, overestimations of 5–8% were found in some of the points. When using the Eclipse TPS for IMRT planning of head and neck cases, the AAA should be used instead of the PBC algorithm, bearing in mind that the AAA may still overestimate the dose near the air–tissue interface when small beam segments are used with the presence of large air cavities.

References

Arnfield M, Siantar C, Siebers J, Garmon P, Cox L and Mohan R 2000 The impact of electron transport on the accuracy of computed dose *Med. Phys.* **27** 1266–73

Bragg C M, Wingate K and Conway J 2008 Clinical implications of the anisotropic analytical algorithm for IMRT treatment planning and verification *Radiother. Oncol.* **86** 276–84

Cheng J, Chao K and Low D 2001 Comparison of intensity modulation radiation therapy (IMRT) treatment techniques for nasopharyngeal carcinoma *Int. J. Cancer* **96** 126–31

Ding G, Duggan D, Lu B, Hallahan D, Cmelak A, Malcolm A, Newton J, Deeley M and Coffey C 2007 Impact of inhomogeneity corrections on dose coverage in the treatment of lung cancer using stereotactic body radiation therapy *Med. Phys.* **34** 2985–94

Epp E R, Boyer A L and Doppke K P 1977 Underdosing of lesions resulting from lack of electronic equilibrium in upper respiratory air cavities irradiated by 10 MV x-ray beams *Int. J. Radiat. Oncol. Biol. Phys.* **2** 613–9

Fu Y T, So P P and Cheung F 2002 Planned stereotactic radiotherapy boost for early T-stage nasopharygeal carcinoma (NPC), experience of Queen Elizabeth Hospital, Hong Kong SAR, China *Int. J. Radiat. Oncol. Biol. Phys.* **54** 171

Gray A, Oliver L D and Johnston P N 2009 The accuracy of the pencil beam convolution and anisotropic analytical algorithms in predicting the dose effects due to attenuation from immobilization devices and large air gaps *Med. Phys.* **36** 3181–91

Hara W, Loo B, Goffinet D, Chang S, Adler J, Pinto H, Fee W, Kaplan M, Fischbein N and Le Q 2008 Excellent local control with stereotactic radiotherapy boost after external beam radiotherapy in patients with nasopharyngeal carcinoma *Int. J. Radiat. Oncol. Biol. Phys.* **71** 393–400

Hunt M *et al* 2001 Treatment planning and delivery of intensity-modulated radiation therapy for primary nasopharynx cancer *Int. J. Radiat. Oncol. Biol. Phys.* **49** 623–32

Jenkins M, Nelson W R and Rindi A 1988 *Monte Carlo Transport of Electrons and Photons* (New York: Plenum)

Kam M K, Chau R M, Suen J, Choi P H and Teo P M 2002 Intensity-modulated radiotherapy in nasopharyngeal carcinoma: dosimetric advantage over conventional plans and feasibility of dose escalation *Int. J. Radiat. Oncol. Biol. Phys.* **56** 145–57

Martens C, Reynaert N, De Wagter C, Nilsson P, Coghe M, Palmans H, Thierens H and De Neve W 2002 Underdosage of the upper-airway mucosa for small fields as used in intensity-modulated radiation therapy: a comparison between radiochromic film measurements, Monte Carlo simulations, and collapsed cone convolution calculations *Med. Phys.* **29** 1528–35

Nelson W R and Jenkins T M 1988 Geometry methods and packages *Monte Carlo Transport of Electron and Photons* (New York: Plenum) chapter 17

Rogers D W O and Mohan R 2000 Questions for comparison of clinical Monte Carlo codes *13th ICCR Monte Carlo Session* http://www.irs.inms.nrc.ca/papers/iccr00/iccr00.html.

So P P, Fu Y T, Yau S and Cheung F Y 2002 Stereotactic radiotherapy boost for nasopharyngeal carcinoma patients with persistent local disease after primary external radiotherapy, experience of Queen Elizabeth Hospital, Hong Kong SAR, China *Int. J. Radiat. Oncol. Biol. Phys.* **54** 286

Sterpin E, Tomsej M, De Smedt B, Reynaert N and Vynckier S 2007 Monte Carlo evaluation of the AAA treatment planning algorithm in a heterogeneous multilayer phantom and IMRT clinical treatments for an Elekta SL25 accelerator *Med. Phys.* **34** 1665–77

Tillikainen L, Helminen H, Torsti T, Siljamaki S, Alakuijala J, Pyyry J and Ulmer W 2008 A 3D pencil-beam-based superposition algorithm for photon dose calculation in heterogeneous media *Phys. Med. Biol.* **53** 3821–39

Van Esch A, Tillikainen L, Pyykkonen J, Tenhunen M, Helminen H, Siljamäki S, Alakuijala J, Paiusco Marta, Iori M and Hutskens D 2006 Testing of the analytical anisotropic algorithm for photon dose calculation *Med. Phys.* **33** 4130–48

Yau T K, Sze W M, Lee W M, Yeung M W, Leung K C, Hung W M and Chan W I 2004 Effectiveness of brachytherapy and fractionated stereotactic radiotherapy boost for persistent nasopharyngeal carcinoma *Head Neck* **26** 1024–30